Live-cell microscopy – tips and tools

Melanie M. Frigault[1], Judith Lacoste[2,3], Jody L. Swift[4] and Claire M. Brown[2,*]

[1]Molecular Oncology Group, McGill University Cancer Centre, Montreal, Canada
[2]McGill University Life Sciences Complex Imaging Facility, Department of Biochemistry, Montreal, Canada
[3]Cell Imaging and Analysis Network, Department of Biology, McGill University, Montreal, Canada
[4]Department of Chemistry, McGill University, Montreal, Canada
*Author for correspondence (e-mail: claire.brown@mcgill.ca)

Journal of Cell Science 122, 753-767 Published by The Company of Biologists 2009
doi:10.1242/jcs.033837

Summary

Imaging of living cells and tissue is now common in many fields of the life and physical sciences, and is instrumental in revealing a great deal about cellular dynamics and function. It is crucial when performing such experiments that cell viability is at the forefront of any measurement to ensure that the physiological and biological processes that are under investigation are not altered in any way. Many cells and tissues are not normally exposed to light during their life cycle, so it is important for microscopy applications to minimize light exposure, which can cause phototoxicity. To ensure minimal light exposure, it is crucial that microscope systems are optimized to collect as much light as possible. This can be achieved using superior-quality optical components and state-of-the-art detectors. This Commentary discusses how to set up a suitable environment on the microscope stage to maintain living cells. There is also a focus on general and imaging-platform-specific ways to optimize the efficiency of light throughput and detection. With an efficient optical microscope and a good detector, the light exposure can be minimized during live-cell imaging, thus minimizing phototoxicity and maintaining cell viability. Brief suggestions for useful microscope accessories as well as available fluorescence tools are also presented. Finally, a flow chart is provided to assist readers in choosing the appropriate imaging platform for their experimental systems.

Supplementary material available online at
http://jcs.biologists.org/cgi/content/full/122/6/753/DC1

Key words: CLSM, Multi-photon, TIRF, Live-cell imaging, Spinning disk

Introduction

Live-cell microscopy has been accessible for decades, as is evident from a movie that was taken with 16-mm film over 50 years ago of a neutrophil chasing a bacterium (David Rogers, Vanderbilt University, http://www.biochemweb.org/neutrophil.shtml). The technique now spans all fields of the life sciences and extends to the physical sciences as well. In recent years, technological advances, including sensor sensitivity, computing power, brighter and more-stable fluorescent proteins (FPs), and new fluorescent probes for cellular compartments, have given researchers the tools to study complex biological processes in great detail (Goldman and Spector, 2005). However, expertise in the optimization of image-acquisition conditions for various microscopy platforms is required to harness the full potential that live-cell microscopy offers.

As with any measuring device, it is best to minimize any perturbations by optimizing the system so that it is minimally invasive. As part of their normal life cycle, most tissues and cells are never exposed to light, and it is known that ultraviolet (UV) light damages DNA, focused infrared (IR) light can cause localized heating, and fluorescence excitation causes phototoxicity to tissues and cells (Pattison and Davies, 2006). The main cause of phototoxicity in living cells is the oxygen-dependent reaction of free-radical species, which are generated during the excitation of fluorescent proteins or dye molecules with surrounding cellular components. Thus, for live-cell imaging, it is best to reduce the amount of excitation light by optimizing the efficiency of the light path through the microscope, and by using detectors that are optimized to detect most of the fluorescence emission. Low concentrations of fluorescent probes also need to be used to avoid causing nonspecific changes to the biological processes of interest.

With live-cell microscopy, there must be a compromise between acquiring beautiful images and collecting data that provide a high enough signal-to-noise ratio (S/N) to make meaningful quantitative measurements of a living specimen. Therefore, the focus of this Commentary is to discuss how to keep cells or tissue alive and healthy during image acquisition, to provide guidelines for different types of samples to delineate the different imaging modalities that are most appropriate, and to provide general and imaging-platform-specific recommendations for instrument components and settings.

A certain level of knowledge about transmitted-light microscopy and fluorescence microscopy is assumed. For the beginner, there are good articles on light microscopy (Murphy, 2001), fluorescence microscopy (Brown, 2007; Lichtman and Conchello, 2005; Murphy, 2001; North, 2006; Wolf, 2007) and confocal microscopy (Hibbs, 2004; Mueller, 2005; Pawley, 2006) that provide the necessary background. There are also many excellent publications on live-cell imaging that provide a lot of detailed and valuable information (Dailey et al., 2006; Day and Schaufele, 2005; Goldman and Spector, 2005; Haraguchi, 2002; Wang et al., 2008) (http://cshprotocols.cshlp.org/cgi/collection/live_cell_imaging). Image analysis is also a crucial component of live-cell imaging, but is beyond the scope of this article. Therefore, the reader is referred to other papers for more details on performing accurate colocalization measurements (Bolte and Cordelieres, 2006; Comeau et al., 2006; Kraus et al., 2007) and accurately quantifying fluorescence signals (Brown, 2007; Cardullo and Hinchcliffe, 2007; Murray, 2007; Swedlow, 2007; Wolf et al., 2007). The focus here is on imaging mammalian cells; however, most aspects of this discussion carry over to the imaging of any living organism or tissue.

Journal of Cell Science

Specimen environment

To successfully image cellular processes in living cells, the cells must be kept in an environment that does not induce stress responses, which can alter the cellular processes of interest. Some of the key factors to consider are the type of culture medium and its contents, and the temperature of the sample, which must be kept stable at 37°C for mammalian cells. Moreover, the pH of the sample must be maintained at a physiological level and evaporation of the medium must be minimized to avoid changes in osmolarity.

Media

For mammalian cells, bicarbonate-based culture medium requires CO_2 to maintain physiological pH. If cells are grown in complete medium containing 10% fetal bovine serum (FBS) in a 5% CO_2 environment, they proliferate and grow; however, they do not survive following the removal of CO_2 (Fig. 1A,E; supplementary material Movie 1), and cell death occurs even more rapidly when serum is not present in the medium (Fig. 1B,E; supplementary material Movie 2). Cell proliferation will continue, however, following the removal of CO_2 if the complete medium is buffered at pH 7.4 with 25 mM HEPES (Fig. 1C,E; supplementary material Movie 3). Notably, after approximately 10 hours without CO_2, the cells in HEPES-buffered medium begin to die (not shown). Cells remain viable in Leibowitz CO_2-independent medium, but they do not proliferate (Fig. 1D,E; supplementary material Movie 4). These experiments emphasize that the presence of carbonate is important for many cellular processes, such as those related to the actions of Cl^- and Na^+ exchangers, as well as co-transporters (Kanaan et al., 2007), and is not simply required

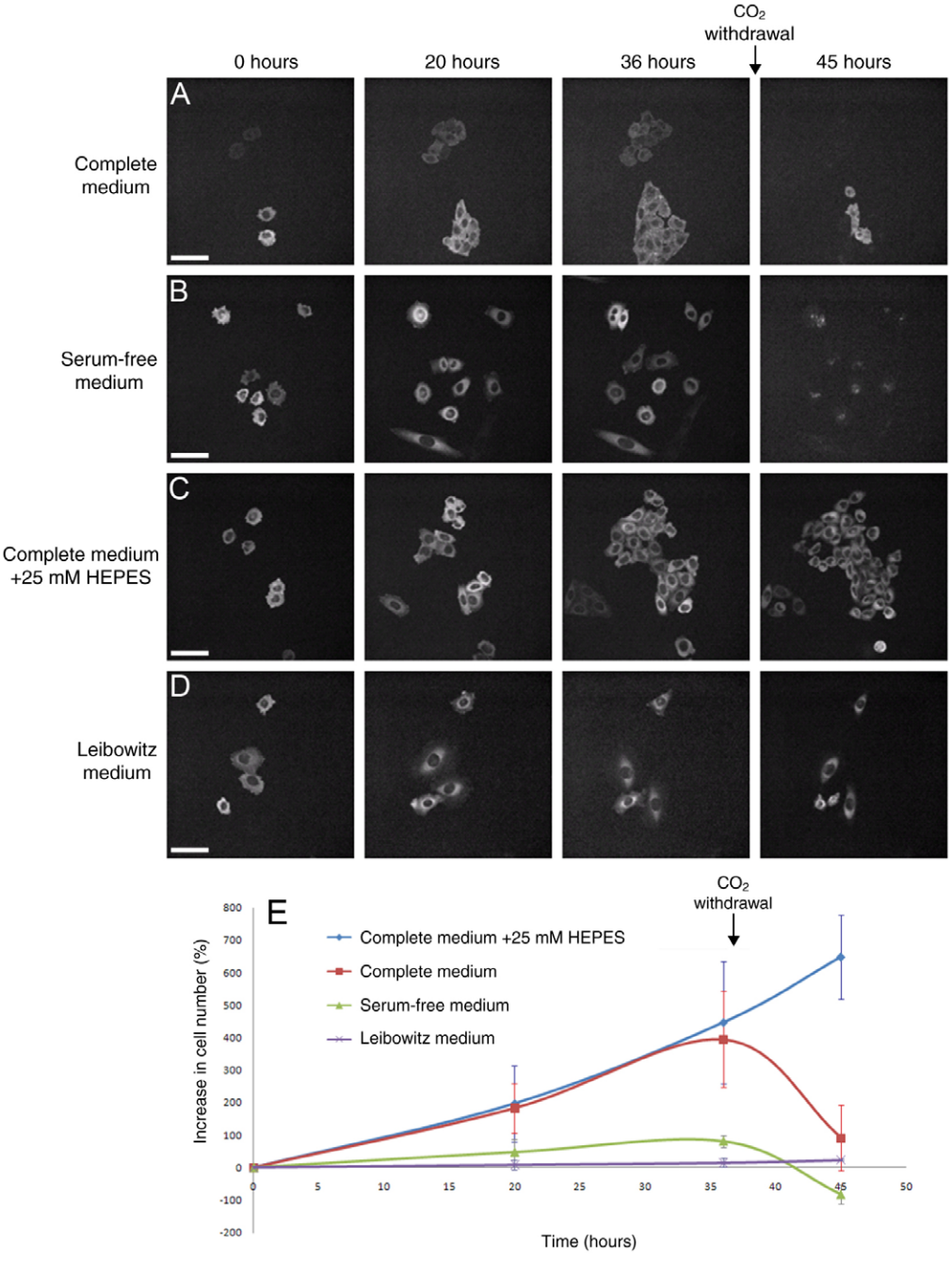

Fig. 1. Effects of the type of medium and the presence or absence of CO_2 on cell proliferation. CHO-K1 paxillin-EGFP-expressing cells were plated on 2 μg/ml fibronectin-coated Lab-Tek II (Thermo Fisher Scientific, NY) eight-well chamber cover-glass slides 24 hours before imaging. Cells were maintained at 37°C in a Chamlide TC system (Live Cell Instruments, Seoul, Korea) with 5% humidified CO_2. (A) Complete Dulbecco's modified Eagle's medium (DMEM) (10% FBS). (B) Serum-free DMEM. (C) Complete DMEM supplemented with 25 mM HEPES. (D) Leibowitz medium (CO_2-independent) with 10% FBS (Gibco). (A-D) Images were collected on a WaveFX SD-CM (Quorum Technologies, Guelph, ON) mounted on a Leica (Wetzlar, Germany) DMI6000B motorized microscope with a 20× (0.7 NA) DIC oil-immersion lens, a custom-modified Yokogawa CSU10 head and a Synapse Diode Laser merge module. EGFP was excited with ~30% of a 25 mW, 491-nm line, using a custom 440/491/561/638 dichroic mirror and a 520/35-nm band-pass (BP) filter. Images were collected with 400-ms exposure times with a Hamamastu (Shizuoka, JP) C9100-12 EM-CCD camera. Maximum projections of seven images of *z*-planes 0.3 μm apart are shown for each time point. Brightness, gamma and contrast were adjusted to the same settings for all images within a given panel. (E) Plot of cell growth relative to the initial time point for the four different types of culture media; error bars represent s.d. for three image fields. Scale bars: 50 μm.

to buffer the medium (Casey, 2006). All media should be supplemented with 25 mM HEPES to avoid adverse effects on cells due to pH changes, which can occur after approximately 5 minutes in the absence of CO_2 (not shown). Incubation chambers can be used with a simple pressure regulator attached to a tank of 5% CO_2 balanced with air. More expensive gas mixers using pure CO_2 can be used and will provide more flexibility in regulating gas concentrations.

Temperature

Large boxes that enclose the whole microscope or smaller stage-top incubators are commercially available. Large microscope enclosures can offer superior temperature stability, as the entire microscope is heated. However, these systems take a long time to stabilize (>12 hours), can be cumbersome to work on, might require expensive custom modifications when upgrading microscope components, and cause significant room heating. Stage-top incubation chambers of various designs can accommodate single 35-mm dishes, multi-well slides and multi-well plates, and many include options for perfusion and electrophysiology. When using stage-top incubators with immersion objectives, an objective heater is essential. The immersion objective acts as a heat sink, resulting in a lower temperature in the field of view where the objective and sample make contact. It is best to remove all other objectives from the microscope turret as they create a large thermal mass that needs to be heated. Most focus drift is due to changes in air temperature, so microscopes should be kept away from air conditioning or heating vents. Any vents in the room should be covered with HEPA filters to diffuse air and remove dust. More detailed information on live-cell chambers is available elsewhere (http://www.microscopyu.com/articles/livecellimaging/culturechambers.html; http://www.olympusfluoview.com/resources/specimenchambers.html). On a tight budget, incubation chambers can be made out of cardboard, insulating packing material and an egg-incubator heater (http://cshprotocols.cshlp.org/cgi/content/full/2007/14/pdb.prot4792).

Osmolarity

To avoid changes in osmolarity caused by evaporation of the medium, it is necessary to humidify the air over the sample. Typically, the CO_2 gas is bubbled through a water reservoir to humidify the environment. When using large chambers that enclose the entire microscope, only a small enclosure placed over the specimen should be humidified so that moisture does not damage the mechanical parts of the microscope.

Monitoring cell health

Cell migration or proliferation can be monitored without the need for fluorescence illumination or the insertion of probes. Thus, these cellular processes, as well as fluorescent and non-fluorescent cell-viability indicators, can be used to monitor the general health of cells. More subtle perturbations might not be readily visualized simply by looking at the cells; therefore, dyes that determine cellular metabolic activity, such as alamarBlue (Invitrogen), can be used. In general, cell health should always be monitored, even following fluorescence imaging, to observe any possible delayed phototoxic effects. It is important to avoid the following conditions before conducting live-cell experiments.

Cell death or stress

Monitoring cell morphology using transmitted-light microscopy techniques [e.g. differential interference contrast (DIC) or phase contrast] can quickly identify cells that are stressed, dying or dead. If cells are forming many irregular plasma-membrane bulges (commonly referred to as blebbing), have many large vacuoles or are detaching from the tissue-culture plate, they are under stress and probably in some stage of necrosis or apoptosis (http://www.microscopyu.com/articles/livecellimaging/livecellmaintenance.html).

Clustering of fluorescent proteins

FP clustering is a strong indication that cells are under stress (http://www.microscopyu.com/articles/livecellimaging/livecellmaintenance.html). The clustering could be a stress response itself, or the stress could be caused by overexpression of the proteins, which then cluster. In general, protein expression levels should be kept as low as possible. RNAi knockdown of endogenous proteins followed by expression of FP constructs by an inducible promoter is recommended to ensure physiological levels of protein expression. One strategy to ensure low expression of FPs is to keep the total DNA concentration constant (e.g. 1 μg/ml) while diluting the FP-specific plasmid by up to 90% with a prokaryotic expression plasmid that does not contain an FP – for example, 0.1 μg of the FP plasmid and 0.9 μg of a Bluescript vector in 1 ml of transfection reagent.

Enlarged mitochondria or broken mitochondrial network

Healthy cells have a very dynamic mitochondrial network. During apoptosis, this network collapses into more numerous, enlarged and isolated mitochondria (Suen et al., 2008). Cell health can thus be monitored using live-cell stains such as the MitoTracker dyes (Invitrogen).

Cellular contamination

Contamination of cells with bacteria, mold or yeast can be visualized when imaging cells (http://www.microscopyu.com/articles/livecellimaging/livecellmaintenance.html). Conversely, mycoplasma are hard to detect visually so it is best to check all cells in the laboratory for mycoplasma contamination on a regular basis (every 3-6 months) using commercially available PCR-based detection kits. If contamination exists, it is best to obtain new stocks of cells, although drugs (e.g. Ciprofloxacin) are also available to decontaminate precious cell lines.

Image acquisition

The key to live-cell fluorescence microscopy is to collect as much fluorescent light as possible so that incident light can be decreased, thereby reducing phototoxic effects. This goal can be achieved by implementing the following three measures. First, it is necessary to improve the efficiency of the optical light path of the microscope. Second, optimizing the detector S/N will ensure that as much light as possible is detected. Third, with an efficient microscope and sensitive detector, the amount of excitation light that is applied to the sample can be minimized. Ways to apply these three measures will be discussed in the following sections and are summarized in Table 1.

Platform-independent optimization

Excitation and emission filters and beam-splitting dichroic mirrors are key components of any fluorescence microscope, and are often assembled into a fluorescence filter cube for specific dyes or dye combinations. Excitation and emission filters can also be placed in filter wheels to automate changes between different excitation and emission wavelengths. For confocal microscopes, these three components are typically mounted on wheels within the confocal head. An easy and relatively affordable way to improve the efficiency of light throughput on any microscope is to replace older,

Table 1. Suggested optimal settings and starting points for imaging on various platforms*

Platform	To improve efficiency	To improve sensitivity and S/N	To minimize light exposure
All	Hard-coated filters (see Box 1). Dye-specific filters. Avoid excess optical elements (lenses, DIC components). 100% light to detector port. High NA objectives. Spectral un-mixing. Avoid phase objectives.	**General:** Phenol-red-free medium. Restorative deconvolution. **Camera-based systems:** Avoid color cameras. Bin high-resolution cameras 2×2 (exposure times of 200-500 ms). Slow camera read times. Use EM-CCD for high speed (exposure times of <100 ms).	Keep excitation light levels low. Avoid blue dyes. Minimum resolution (60×, 1.4 NA): *x,y* ~0.1-0.2 μm *z* ~0.3-0.4 μm *t*=2.3× timescale of events. Minimum number of probes. Use oxygen-radical scavengers.
WFM	Remove DIC prism and analyzer when imaging fluorescence.	Perform post-acquisition restorative deconvolution (Fig. 3C,D).	Find cells with transmitted light. Use ND filters (<10% lamp power). Use UV- and IR-blocking filters. Use halogen lamps if possible.
CLSM	Use long-pass or wide band-pass filters and un-mix post acquisition. Open the pinhole ≥2 Airy units. Remove DIC prism.	High PMT voltage (≥800 V). Restorative deconvolution. Avoid spectral-array detectors.	Low laser power. AOTF laser blanking. No line or frame averaging. Fast scan speed (≥8 μs/pixel). Image regions of interest when possible. Recommended laser powers: 405 nm Avoid 488 nm <2% (30 mW) 514 nm <2% (30 mW) 543 nm <50% (1 mW) 633 nm <5% (5 mW)
MP-CLSM	Use long-pass filters and un-mix post acquisition. Use NDDs.	Use high PMT voltages. NIR light is lower in energy. Restorative deconvolution.	Refer to points for CLSM above. Inherently confocal excitation. One excitation for multiple dyes. For a 2 W multi-photon laser recommend ~2 mW (<10 mW) at 860 nm for cellular work. Higher powers are needed for intravital imaging deep inside tissue.
SD-CM	Most current confocal heads (Yokogawa X1) or optimized versions of the Yokogawa CSU-10 (e.g. Quorum Technologies). Use high-quality high-light-throughput camera-coupling lenses.	Choose appropriate camera for resolution (scientific grade CCD) or speed (EM-CCD). Restorative deconvolution (Fig. 5C,D).	Keep laser power low. Excitation light spread over thousands of pixels. Excitation light is confocal. Recommended laser powers: 405 nm Avoid 440 nm <70% (15 mW) 491 nm <30% (25 mW) 561 nm <20% (50 mW) 638 nm <20% (30 mW)
TIRFM	Use broad band-pass or long-pass filters. TIRF filters to avoid laser reflections and interference patterns.	Choose appropriate camera for resolution or speed. Little out-of-focus light.	Only excite probes ~100 nm from cover-slip surface. Recommended laser powers: 405 nm Avoid 488 nm <20% (30 mW) 514 nm <20% (30 mW) 543 nm ~50-100% (1 mW) 633 nm <20% (5 mW)

*Note that these are only suggestions and the actual values will depend on the specific microscope, lenses, dyes, tissue and detectors. These settings are meant as a guideline, but all settings should be optimized further for each piece of equipment with specific samples under given experimental conditions.

soft-coated excitation and emission filters and dichroic mirrors with new, hard-coated filters and mirrors (Box 1). Hard-coated filters have stable coatings that are not sensitive to heat and humidity, and they offer a 20-30% increase in light throughput when compared with soft-coated filters (Standish, 2008). For single-color experiments, use excitation and emission filters, and a dichroic mirror that is optimized for the specific dye. For example, when imaging red fluorescent protein (RFP), do not use filters and mirrors that are optimized for rhodamine. Additional surfaces in the light path, such as DIC optics or optivar lenses, should be avoided, and the microscope should be configured to allow 100% of the light to go to the detection port.

For multi-color experiments, it is better to use filters and mirrors that are designed for single dyes, and to collect images sequentially to optimize the light collection for each fluorophore. However, care must be taken because slight variations in mounting positions between different mirrors can result in shifts in image focus and *x,y* locations between images of different colors, making colocalization measurements difficult. Multi-chroic mirrors avoid these shifts and are required when imaging rapid cellular processes (on a timescale of <1 minute), but light-collection efficiency is reduced, sometimes significantly. For example, when imaging enhanced green fluorescent protein (EGFP) and RFP, the mirror must reflect green light onto the specimen to excite RFP fluorescence; however, the mirror will also reflect much of the green fluorescence from the EGFP emission, so this will go undetected, thereby reducing the sensitivity of the system.

For multi-color experiments, it is essential to collect images in all detection channels for control samples that contain only one dye. By imaging these samples under the exact same conditions as multi-labeled samples, crosstalk (excitation of one dye by the incident light intended for another dye) and bleed-through (emission of one dye into the detection channel of another dye) in the images can be corrected for (Kraus et al., 2007). For example, if EGFP and RFP are being imaged simultaneously, some of the EGFP signal will be collected in the RFP image, so this contribution should be measured using a sample with only EGFP and re-assigned back to the EGFP image. Avoid using phase objectives or DIC optics while imaging fluorescence because the phase ring, the DIC prism and the analyzer all reduce the light-collection efficiency.

The efficiency (*E*) of light collection by lenses is proportional to the numerical aperture (*NA*) and the magnification (*Mag*) of the lens, and is defined as:

$$E \propto \frac{NA^4}{Mag^2} . \quad (1)$$

Thus, high NA lenses are crucial for live-cell imaging because small changes in NA result in significant improvements in light collection. However, increases in magnification decrease light-collection efficiency. Therefore, a 60×, 1.4 NA lens will collect considerably more light than a 100×, 1.4 NA lens (http://www.microscopyu.com/articles/livecellimaging/imagingsystems.html).

To improve the S/N, nonspecific background intensity can be reduced by using phenol-red-free medium. Images of live cells typically have a low S/N, and do not use the full dynamic range of the camera (typically ⩽20%) because of the need to reduce phototoxicity. Nonetheless, the S/N must be high enough to observe or measure the biological processes of interest. For camera-based systems, the choice of camera will depend on the application. For transmitted-light microscopy, affordable complementary metal-oxide semiconductor (CMOS) cameras are ideal, whereas high-resolution scientific-grade charge-coupled device (CCD) sensors (e.g. Sony ICX-285 chip) (Box 1) should be used for most fluorescence applications. These CCDs detect about 60-70% of the photons that reach the detector – that is, they have a quantum efficiency (QE) of 60-70% across the visible-light spectrum. These CCD arrays give high-resolution images

Box 1. Microscope accessories for live-cell imaging

Lamps

Mercury lamps. Pros: bright light across spectrum, readily available. Cons: UV damage, uneven emission spectra, 200-hour bulbs, heat generation, mercury, intensity decreases over time, bulb alignment.

Halogen lamps. Pros: long-life cheap bulbs, no UV damage, no bulb alignment. Cons: not very bright.

Metal halide lamps. For example, Chroma Technologies, Photofluor; EXFO Life Sciences, X-cite; Zeiss, Illuminator HXP 120. Pros: uniform emission spectra, 2000-hour bulbs, no alignment, intensity stable over time. Cons: UV component, expensive liquid-light guides.

Light-emitting diodes (LEDs). For example, Zeiss, Colibri; COOLED, PrecisExcite. Pros: last for 10,000 hours, fast electronic switching between colors, discrete excitation bands, no heat generated, no UV damage. Cons: expensive up-front cost, missing wavelengths, only 3-4 wavelengths available at a time.

Filters

Hard-coated filters can increase light throughput by 20-30% (Chroma Technologies, ET Series; Semrock, Brightline; Omega Optical, QMAX) when compared with traditional soft-coated filters.

Shutters

Required for time-lapse experiments unless using LED light sources. Can be built in (Zeiss, Axiobserver) or added between the light source and the microscope (Sutter, Prior).

Autofocus

Focus drift is a key problem with live-cell imaging. Image-based autofocus is not recommended; laser-based autofocus is best.

Motorized stage

Parallel experiments optimize resources and are useful for long time-lapse experiments. Linear-encoded stages should be used.

Cameras

Color and CMOS should be avoided. High-resolution CCD (Sony, 285 chip; Photometrics, CoolSNAP; QImaging, RetigaExi; Hamamatsu, ORCA-ER) is recommended if time is not an issue (>100 ms exposure). For speed, a back-thinned EM CCD sensor is needed and high-quality coupling optics for the 512×512 array should be used to meet the Nyquist sampling criterion. New back-thinned 1000×1000 array sensors (Hamamatsu, ImageEM-1K; Photometrics, Cascade II-1024; Andor Technology, LucaEM) have a higher resolution, but coupling to meet the Nyquist sampling criterion for SD-CM must be done properly.

Spectral detectors

Used to image many dyes simultaneously or remove autofluorescence. Fast PMT array detectors are recommended (e.g. Zeiss, 510 Meta), but there is a loss in sensitivity when compared with PMT detection. Newer array detectors have much better sensitivity. Slit-based spectral imagers (e.g. Olympus, FV1000) are more sensitive and have higher spectral resolution, but are slow and not ideal for live-cell time-lapse imaging.

(~0.1 μm pixels at 60×) so the camera can be 'binned' by adding together pixel arrays to increase the S/N, allowing for shorter exposure times, albeit at the expense of some spatial resolution (Brown, 2007) (http://www.microscopyu.com/articles/livecellimaging/imagingsystems.html). Back-thinned electron-multiplied (EM)-CCDs are highly sensitive with a QE of ~90% across the visible-light spectrum. By activating a gain register on the CCD chip, EM gain on these cameras can be turned on, which amplifies the signal up to 1000-fold, although noise will also be amplified. These cameras are ideal for high-speed imaging (<100 ms exposure times), but care should be taken that the EM gain is optimal for an increased S/N without detector saturation. Notably, EM-CCDs typically have lower spatial resolution than the standard scientific-grade CCDs (512×512 pixel array sensors have ~0.3 μm pixels at 60×). Reduce noise by using the slowest camera read speed available. For more information on CCD cameras and companies see the following references (Nordberg and Sluder, 2007; Spring, 2007) and website (http://micro.magnet.fsu.edu/primer/resources/digital.html).

Image deconvolution can considerably improve the S/N and spatial resolution of images post-acquisition. A microscope image is a representation of an object generated from the convolution of the optical elements of the microscope, with the light emitted by or transmitted through that object. Light from a point source within a fluorescence image is spread out in *x*, *y* and *z*, making the point source appear larger than it really is. The size of the point source will depend on the resolving power of the microscope objective, the detector resolution and the color of the emitted light. Image deconvolution relies on algorithms to restore the image so that it is a more accurate representation of the actual object, as though the light was not distorted by the microscope optics. There are two main types of deconvolution – non-quantitative and quantitative. Non-quantitative techniques (e.g. nearest neighbor) use subtraction algorithms that estimate and remove light that was spread out by the optics. The image S/N increases but sensitivity is lost, and images are no longer quantitative (Swedlow, 2007; Wallace et al., 2001). Quantitative restorative image deconvolution relies on extensively developed algorithms that use an iterative process to mathematically reverse the blurring effects of the optics so that captured light is reassigned to its true point of origin. In this way, the S/N of the image is significantly increased and quantification of fluorescence is retained while generating higher resolution images (Holmes et al., 2006; McNally et al., 1999; Murray, 2005; Shaw, 2006; Swedlow, 2007; Wallace et al., 2001) (http://micro.magnet.fsu.edu/primer/digitalimaging/deconvolution/deconvolutionhome.html). Well-established commercial software packages that use algorithms to generate quantitative images are available for performing restorative deconvolution, such as Huygens software (Scientific Volume Imaging), Zeiss Axiovision and AutoQuant X (Media Cybernetics). Image deconvolution requires the collection of a *z*-stack of images, so for live-cell applications it should only be used if three-dimensional (3D) information is required. Placing sub-resolution 0.1 μm beads on the cells can be used to test for proper image restoration. Examples of deconvolution for specific platforms will be given in the sections below.

For any light source, the power must always be minimized, and dyes that require UV excitation should be avoided. For instance, nuclear labeling with blue Hoechst dye can be substituted with the far-red dye Draq5 (Biostatus Ltd); nevertheless, care should be taken with nuclear dyes as they rarely allow normal cell division to occur.

Minimal lateral (*x* and *y* axes) and axial (*z* axis) resolution should be used to see the structures of interest. The Nyquist criterion states that, in order to accurately reconstruct a signal (e.g. a microscopic object), sampling should be carried out at a spacing ~2.3× smaller than the signal that is being measured (Nyquist, 1928; Pawley, 2006; Shannon, 1949). In light microscopy, the smallest signal that can be measured is the resolution limit of the system, which is determined by the wavelength of light being used and the NA of the lens. The resolution (*R*) of a specific lens is defined as:

$$R = \frac{\lambda}{2NA}\ , \qquad (2)$$

where λ is the wavelength of the emission light. For a 60×, 1.4 NA oil-immersion lens using 500-nm light, the resolution is 0.18 μm. In this case, sampling should be done at 0.078 μm. The Nyquist criterion can also be applied for temporal resolution to reconstruct dynamic events of interest. For example, if an event takes hours, samples should be taken every 20-30 minutes, as resolution on the scale of minutes or seconds is not required.

Use the minimum number of fluorescent probes that are required, thereby avoiding excess light exposure and reducing the potential for probes to produce non-physiologically relevant responses and stresses. Oxygen-radical scavengers can be used to minimize photobleaching and phototoxicity, but should not affect cell viability, and should be tested for effectiveness with the given fluorescent dye and imaging conditions.

Platform-specific optimization

Transmitted-light microscopy

A great deal of information can be gained simply by observing cells using transmitted-light microscopy techniques such as phase contrast or DIC (Murphy, 2001). Because there is plenty of light available using these techniques, light throughput and the S/N should not be issues; however, regular cleaning of the optical components is required to maintain high image quality. Proper Köhler alignment of the microscope and alignment of phase or Nomarski (DIC) optics are crucial. See your microscope manual or refer to the following websites for further details (http://micro.magnet.fsu.edu/primer/techniques/dic/dicconfiguration.html; http://www.microscopyu.com/articles/phasecontrast/phaseconfiguration.html).

Low levels of white light do not show any obvious adverse effects on cells. However, care should be taken not to use high levels of transmitted light as there are near-UV and near-IR (NIR) components in some white-light sources that, when highly focused by the microscope, can disrupt the cell. It is best to reduce the intensity of the light and increase the camera exposure time to generate high S/N images and minimize any potential adverse effects on the cell.

With transmitted-light microscopy, potential perturbations to cells owing to the introduction of FPs or dyes are avoided. DIC images inherently have some shading, which can be corrected using an image that is collected with no sample on the microscope or when the sample is out of focus. Automated shading-correction algorithms are often included in microscope software packages and involve the original DIC image (Fig. 2A,A′) being divided by the shading image (Fig. 2B), resulting in a corrected image (Fig. 2C,C′). From time-lapse DIC movies (Fig. 2D; supplementary material Movie 5), processes such as cell proliferation (Fig. 2E), migration (Fig. 2F), and the fast movements of organelle and vesicle dynamics (supplementary material Movie 6) can be measured.

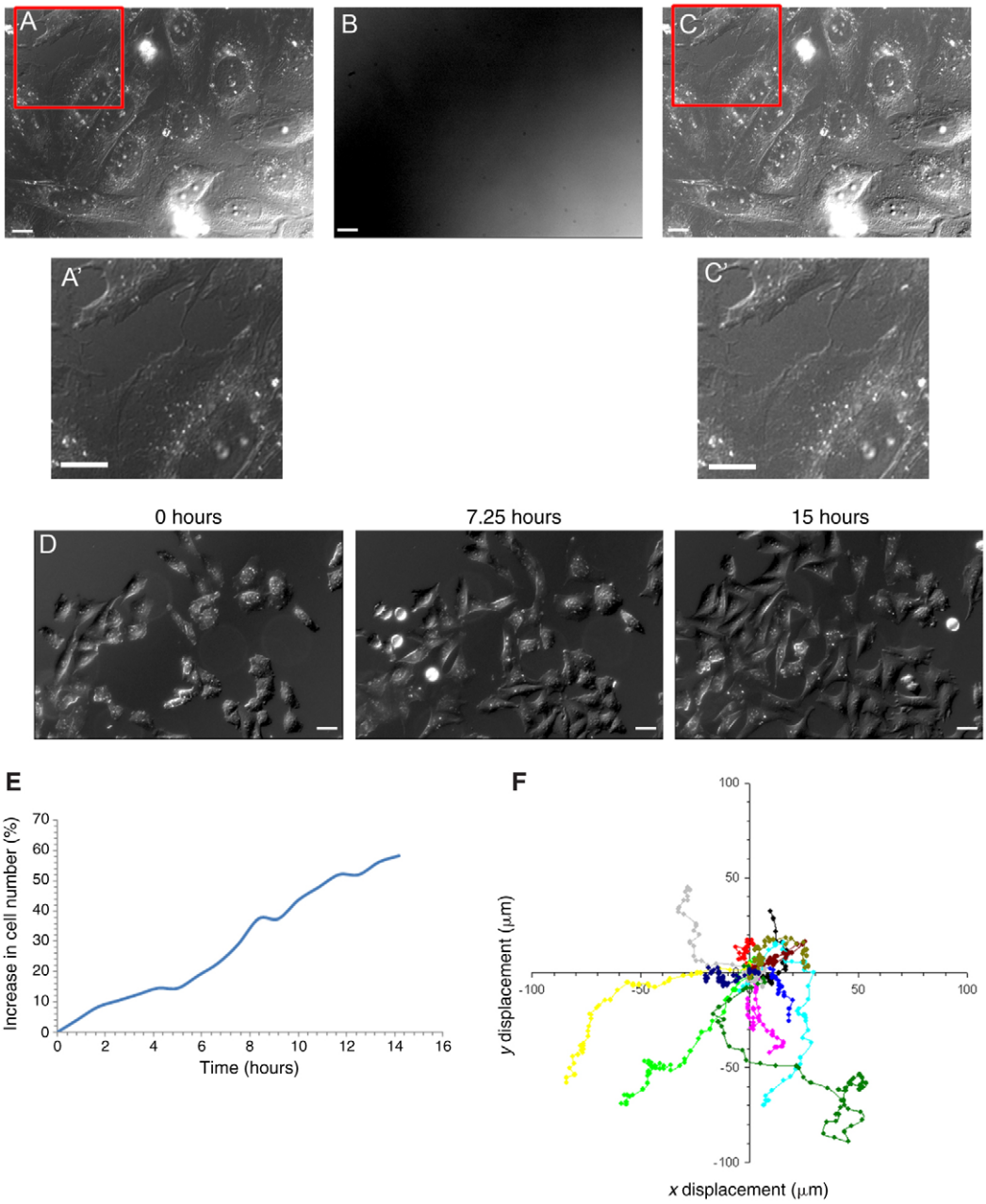

Fig. 2. Cell proliferation and tracking can be measured from bright-field images such as DIC. CHO-K1 cells expressing paxillin-EGFP were plated on 35-mm glass-bottom dishes (World Precision Instruments, Sarasota, FL) coated with 2 μg/ml fibronectin (Sigma-Aldrich) 24 hours prior to imaging. Cells were maintained at 37°C with 5% humidified CO_2 in a Solent Scientific (Segensworth, UK) incubation chamber. DIC images were collected on an Olympus (Tokyo, Japan) IX81 microscope with a 20× (0.4 NA) objective lens, using a Photometrics (Tuscon, AZ) CoolSNAP EZ camera with no binning. Raw images (A,A′) were corrected for shading using the MetaMorph (MDS Analytical Technologies, Sunnyvale, CA) shading-correction algorithm and a shading image collected above the focal plane (B) to give corrected images (C,C′). Areas enclosed by red boxes in A and C are shown at higher magnification in A′ and C′, respectively. Cells were imaged every 5 minutes for 15 hours with a 20× (0.4 NA) objective (D) with 1-second exposure with the halogen lamp at low intensity. Cell numbers were counted manually for cell-proliferation measurements (E), and the manual cell-tracking feature in MetaMorph was used to generate cell tracks for the Rose plot (F). Scale bars: 10 μm.

Wide-field fluorescence microscopy (WFM)

Wide-field fluorescence microscopes are readily available, sensitive, and can be fast, affordable and versatile for live-cell microscopy. Imaging transmitted light in combination with fluorescence should only be done when it is essential, because the ring in phase objectives will block some of the emitted fluorescence light (~15-20%), and the losses through the DIC analyzer (~50%) and prism (10-20%) can result in a combined loss of 50-70% of the fluorescence emission light (Fig. 3A,B). If motorization is available, the DIC components can be removed when imaging fluorescence, maximizing the efficiency of light collection.

In general, wide-field fluorescence microscopes make efficient and affordable 3D-imaging systems that can generate beautiful high-resolution images (Fig. 3C). When looking for protein localization, such as in focal adhesions, WFM is often suitable for long-term and relatively rapid quantitative time-lapse imaging (Webb et al., 2004; Webb et al., 2002). For thin samples, such as cell monolayers, 3D-image stacks can be collected and restorative blind deconvolution can be performed, generating images of high S/N (compare Fig. 3C′ with 3D) and high resolution (compare Draq5 staining in Fig. 3C with that in 3D). Beautiful 3D iso-surfaces can also be generated (Imaris software, Bitplane), emphasizing the improvements in the S/N (compare Fig. 3C′ with 3D) and resolution (compare Fig. 3C with 3D) following deconvolution. Imaris software can also be used to measure fluorescence intensities and volumes, and to track objects in 3D. Nevertheless, 3D imaging should only be used when essential, as it requires many more exposures of the sample to excitation light.

Minimize phototoxicity by focusing on samples using transmitted light. Directly observing cells for 10 seconds with a 100 W mercury bulb at full power destroys ~80% of EGFP fluorescence (Fig. 4A,B; supplementary material Movie 7). This photobleaching makes it

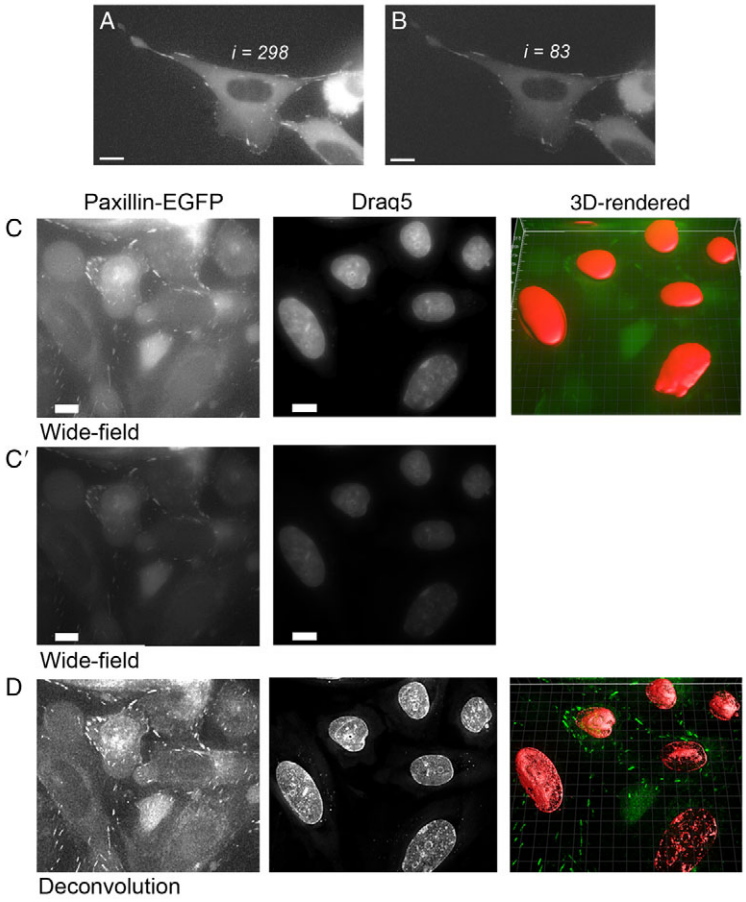

Fig. 3. Loss of light across DIC optics and WFM plus deconvolution increases S/N and resolution. Images of CHO-K1 cells prepared and imaged as in Fig. 2. Fluorescence images of paxillin-EGFP-expressing CHO cells without (A) and with (B) DIC optics (prism and analyzer) in place. Using DIC optics decreases the cellular intensity (*i*) by 72%, from 298 to 83. (C) The same cells labeled with the nuclear dye Draq5 (0.5 μM) were imaged using 6% lamp power. Using a 0.2-μm step size, 241 *z*-planes were collected with 2×2 pixel binning and a 1-second exposure time using a custom triple cube for EGFP-mCherry-Cy5 (Chroma Technology). EGFP was imaged with a 480/20 excitation filter and a 515/30 emission filter, whereas Draq5 was imaged with a 630/30 excitation filter and 685/70 emission filter. Maximum-intensity projections of the raw wide-field images are shown for the central 21 image planes, and contrast, gamma and brightness were adjusted to see the intensity of labeling. (C,D) For intensity comparisons, the same projected images of the raw data are shown (C′) on the same display scale as the deconvolved images (D), but are a bit difficult to see. (D) The native.stk MetaMorph-format files were transferred into the Autoquant X2 deconvolution software (http://www.mediacy.com/index.aspx?page=Home). Each file was subjected to a 20-iteration deconvolution using the 'adaptive blind' deconvolution algorithm starting with the theoretical point spread function. Following this, the deconvolved files were imported directly into the Imaris 6.1.5, 3D/4D Image Analysis software (www.bitplane.com). Rendered 3D iso-surface plots are shown (C,D). Scale bars: 10 μm.

difficult to follow proteins of interest, and causes phototoxicity. Using a neutral density (ND) filter that reduces the lamp power to 6% minimizes the bleaching so that only ~20% of the fluorescence signal is lost after 60 seconds of constant illumination (Fig. 4B,C; supplementary material Movie 8). In addition, even with the best-quality excitation band-pass (BP) filters and dichroic mirrors, some of the UV and IR components of the mercury lamp can still pass to the sample. Additional filters that specifically block UV light, or heat filters for IR light, can also be used, but might not be required if the lamp is attenuated to levels that are acceptable for live-cell imaging (<10%).

Halogen-lamp sources that are designed for transmitted-light microscopy can generate beautiful live-cell fluorescence images (Webb et al., 2004). These lamps are much lower power, have long-lasting mercury-free bulbs, a minimal UV component, are affordable and do not require alignment. However, these lamps might not produce enough light for very dim fluorophores or rapid imaging. Oxygen-radical scavengers such as ascorbic acid have been reported to be good anti-oxidants for live-cell imaging (Knight et al., 2003). Nonetheless, in our hands, scavenger concentrations of 100 μM did not make a significant difference in photobleaching rates under constant illumination (Fig. 4B). This discrepancy could be due to the fact that ascorbic acid is better suited for fluorophores other than EGFP, or perhaps because time is required between successive exposures for any benefit to be observed. Notably, this emphasizes the need to test any additive for functionality under specific experimental conditions.

The exclusion of dyes from cellular compartments can be used to identify cells or structures within the cell. For example, refrain from using a nuclear dye if a protein is absent from the nucleus (Fig. 4D). Images can be inverted and algorithms can find objects on the basis of intensities above a threshold (Fig. 4E), or a morphology filter can be used to find dark (or light) holes in the image (Fig. 4F).

Confocal laser-scanning microscopy (CLSM)

Confocal microscopy is required when working with thick specimens, such as tissue slices and small organisms, to eliminate out-of-focus light (Pawley, 2006). There are many publications on the use of confocal laser-scanning microscopes for live-cell microscopy (Dailey et al., 2006), with some that date back to the early 1990s and describe the measurement of Ca^{2+} waves (Cornell-Bell and Finkbeiner, 1991) or the dynamics of neuronal axons and growth cones (Fraser and O'Rourke, 1990). Nonetheless, it can be challenging to optimize the multitude of CLSM settings when working with living tissue to reduce localized phototoxicity that is caused by the highly focused laser light.

Use long-pass (LP) or wide BP filters when possible, and for multiple dyes correct for crosstalk and bleed-through by post-acquisition processing (Kraus et al., 2007). Similar to WFM, imaging dyes sequentially by using single dichroics provides more sensitivity, but there is a time delay between images or different dyes, and problems with image alignment may arise. Crosstalk and bleed-through of signals between detection channels can be minimized using sequential line scanning so that only one dye is being excited at a time, with the minimum time delay between images. Sensitivity might also be improved by opening up the pinhole (>2 Airy units) at the expense of *z*-axis resolution.

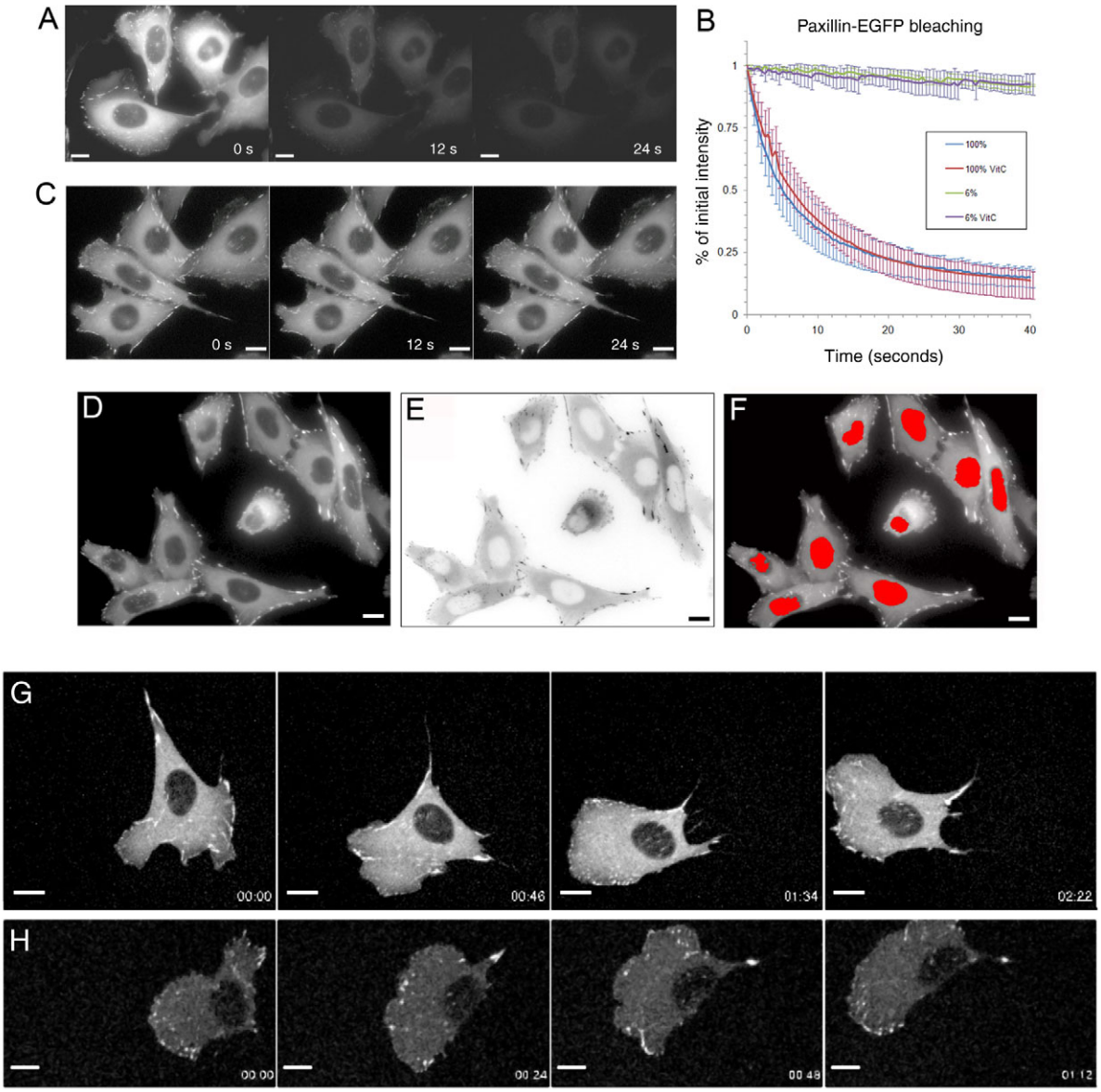

Fig. 4. Lamp photobleaching, image segmentation by absence of fluorescence and CLSM of living cells. Images of CHO-K1 cells prepared and imaged as in Fig. 2. Excitation was from a 100 W mercury lamp using a custom EGFP filter cube for both WFM and total internal reflection fluorescence microscopy (TIRFM) (Chroma Technology, Rockingham, VT, hq480/20×, z488rdc, hq525/50m). Cells were found by using DIC optics. Images using an Olympus 60×, 1.45 NA oil-immersion lens from a time series with 500-ms exposure time using either 100% (A) or 6% (C) power from the lamp. (B) Decrease in cellular intensity for three separate image series measured using a custom journal written for MetaMorph, which measures the intensity of all of the cells in the field of view over time. Error bars are s.d. for the three experiments. (D) Image of paxillin-EGFP expression, which is absent from the nucleus, smoothed using a low-pass filter to remove noise. (E) Image in D inverted to show high intensities and absence of nuclear labeling. (F) A morphology filter was applied using MetaMorph followed by an integrated morphometry analysis (IMA) to select and fill only the large holes. A red mask of the regions of interest detected by the IMA analysis was overlaid on the raw image that is shown in D. Bright focal adhesions below the nucleus can cause some underestimates of the nuclear area (cell on the far left near the bottom of the image). Note that all display properties (brightness, gamma, contrast) have the same settings for images within a panel. (G,H) Confocal images were collected on a Zeiss (Jena, Germany) LSM510 confocal microscope using a 63× Plan-Apochromat 1.4 NA oil-immersion lens. Cells were kept on the stage at 37°C with a Zeiss incubation chamber equipped with a gas mixer and 5% humidified CO_2. Resolution was at zoom one with 0.14 µm in *x* and *y*, and the pinhole was set to 194 µm or ~2.7 Airy units. Six *z*-axis image plans were collected at 0.5-µm separation every 2.5 minutes using 2% of the 488-nm laser (30 mW Ar at 6.0 A current) and a 505 LP emission filter. Two representative cells migrated well under this level of laser-light exposure. A median filter was applied to the images to reduce noise. Scale bars: 10 µm.

Remove the DIC prism because it causes distortions in the images and 10-20% of the fluorescence emission can be lost across this component. It is particularly important to avoid these distortions when performing post-acquisition deconvolution. Thus, only perform DIC and fluorescence CLSM imaging simultaneously when it is absolutely necessary. Moreover, use photomultiplier tubes (PMTs) at high voltage (~800 V) and sacrifice the S/N for sensitivity. Restorative deconvolution is not only for WFM; it can also be used to improve the S/N in CLSM images (Boivin et al., 2005). Avoid spectral-array detectors as they are typically inefficient.

Most modern confocal laser-scanning microscopes are equipped with an acousto-optic-tunable filter (AOTF), which allows for precise attenuation of the lasers. Therefore, start with very low laser

powers and only increase them following optimization of other instrument settings (Table 1). AOTF control also allows the laser to be turned off during the back-scan for uni-directional scanning. Use faster scan speeds (⩾8 μs/pixel) with no line or frame averaging so that the laser spends less time at each pixel. Minimize sampling in *x*, *y* and *z* to reduce the amount of time the focused

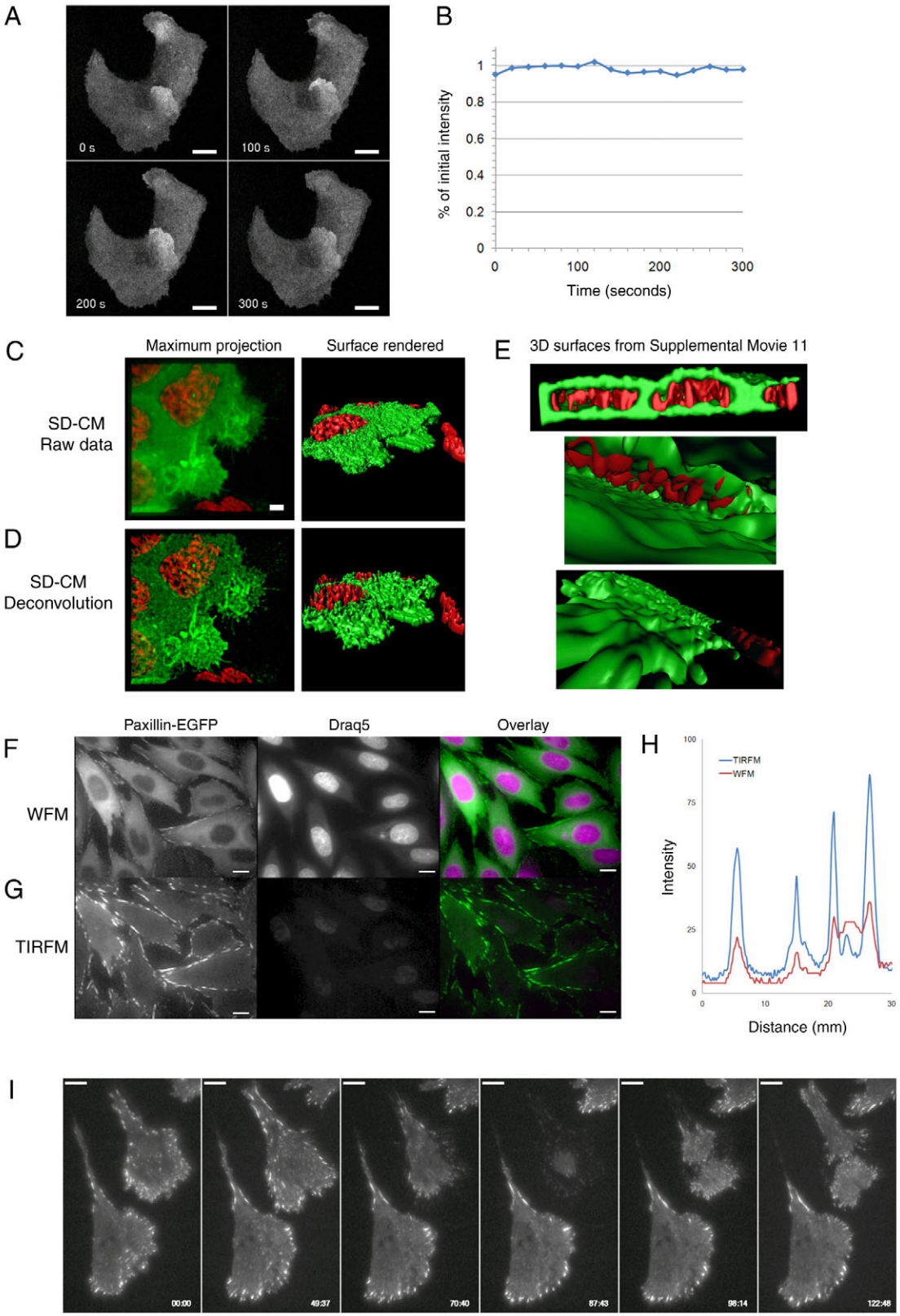

Fig. 5. See next page for legend.

laser beam spends in any location within the sample. If information is only needed in one area of the cell, then image a small region of interest. CLSM can be used to image live cells in 3D for many hours using optimized settings (Fig. 4G,H; supplementary material Movies 9 and 10).

One of the limitations of CLSM is speed; however, there are some strategies that can be used for rapid imaging. Two-color quantitative data at rates of up to 20 frames per second (fps) were achieved for endosomes moving in reticulocytes using small image regions, bi-directional scanning and only scanning every second line along the *y*-axis (Sheftel et al., 2007). Rapid imaging can also be achieved by using repeated line scanning, generating an image of intensity over time for a single line across the specimen (Digman et al., 2008). Spectral-array detectors can be used to collect light of all colors with one pass of the lasers. A lot of light can be lost with these systems, although newer models continue to improve.

Keep in mind that WFM systems can be faster and more sensitive than CLSM systems, as light that is rejected by the pinhole on a confocal microscope is collected on a wide-field microscope. So, for some applications, WFM followed by restorative deconvolution might be more appropriate than CLSM.

Multi-photon confocal laser-scanning microscopy (MP-CLSM)

Multi-photon confocal laser-scanning microscopes are ideal for intravital imaging in thick tissues, in live animals or in tissue-slice cultures (Piston, 2006; Rocheleau and Piston, 2003). Chromatic aberrations are limited with MP-CLSM because, rather than focusing multiple lasers of different colors, a single laser excitation can be used for multiple fluorophores. This makes MP-CLSM ideal for colocalization (Kawano et al., 2008) or co-dynamic measurements such as Förster (or fluorescence) resonance energy transfer (FRET), or two-color image-correlation microscopy (ICM) (Wiseman et al., 2000). Multi-photon fluorescence excitation is based on the simultaneous absorption of more than one NIR photon of light by a single fluorophore molecule. Thus, MP-CLSM is inherently confocal because simultaneous absorption of multiple photons only occurs in the highly photon-dense laser focal volume (Oheim et al., 2006).

Use LP or wide BP filters when possible, and correct for crosstalk and bleed-through with post-acquisition processing (Kraus et al., 2007). The fluorescence emission can be harnessed and detected without going back through the scanning optics [termed non-descanned detectors (NDDs)] because, unlike CLSM, a pinhole is not required. NIR light will also have much less scatter in tissue owing to its long wavelength, so it can penetrate deeply into the specimen with less background fluorescence. Use PMTs at high voltage (~800 V) and, for low-light-level applications, avalanche photodiodes (APDs) can be used. Post-acquisition deconvolution can be performed on 3D multi-photon image stacks.

Fluorescence excitation is limited to the focal volume (~1 fL), reducing overall phototoxicity compared with single-photon CLSM (Schwille et al., 1999). However, there is evidence that localized photobleaching within the focal volume is higher for MP-CLSM (Patterson and Piston, 2000). Therefore, use MP-CLSM for tissue, but single-photon CLSM is better suited for cellular monolayers. Nonetheless, NIR light is of much lower energy than visible lasers and, for multi-color imaging, an NIR laser can excite multiple fluorophores simultaneously. The lowest possible laser power should be used to avoid phototoxicity and any potential heat damage owing to the focused NIR light (Konig, 2006).

With new lasers optimized to generate short, high-energy pulses of NIR light, multi-photon imaging in intact brain is now approaching depths of 1 mm (Helmchen and Denk, 2005). Intravital imaging of FPs combined with probe-free second-harmonic imaging of ordered protein structures, such as collagen fibers, within intact tumors have provided ground-breaking results in breast-cancer research (Yamaguchi et al., 2005). However, keep in mind that MP-CLSM is expensive and requires a lot of expertise, and many dyes have not been characterized so might not be suitable for multi-photon excitation.

Spinning-disk confocal microscopy (SD-CM)

For live-cell microscopy, techniques that spread the illumination light over a larger area of the sample minimize phototoxicity when compared with CLSM (Fig. 5A,B). In addition, data are collected by a CCD array from many sample locations simultaneously for rapid image acquisition. This can be done using a disk that has either slits or thousands of pinholes that allow light to selectively excite fluorescence in multiple regions of the sample. Over time, as the disk spins, the entire specimen is sampled and imaged on a CCD-array detector. Here, we specifically discuss the Yokogawa SD-CM, which uses two disks – one with pinholes and one with micro-lenses – to focus the excitation light into the pinholes, improving the excitation efficiency of the system (Ichihara et al., 1996). There are other designs on the market, which are summarized elsewhere (Toomre and Pawley, 2006).

Use the most current generation of confocal heads (e.g. Yokogawa X1), or systems modified with custom mirrors, dichroics and camera-coupling optics to increase light throughput and

Fig. 5. SD-CM and total internal reflection fluorescence microscopy (TIRFM). MDCK cells expressing EGFP-Gab1 were seeded 1 day prior to imaging on a 35-mm glass-bottom dish (MatTek Corp.) in complete DMEM. Cells were imaged live by SD-CM as in Fig. 1 with a 63× oil-immersion objective. Images were acquired in *z*-stacks of 28 planes at 0.3-µm intervals with 400-ms exposure times every 20 seconds over a period of 30 minutes. (A) Images at the indicated time points of one *z*-plane are shown. (B) Percentage intensity of the two cells shown in A over time. (C,D) Cells were stained with the nuclear dye Draq5 (0.5 µM) and a *z*-stack of 61 planes at 0.2 µm was acquired 15 minutes after treatment with hepatocyte growth factor (HGF; 100 ng/ml). Exposure times were 400 ms and camera gain was set to 203-243. Draq5 was imaged using 69% of the 30 mW, 638-nm laser line, whereas EGFP-Gab1 was imaged using 63% of the 25 mW, 491-nm laser line. The raw data (C) and deconvolved data (D) are shown as maximum projections and 3D rendered iso-surfaces (Bitplane). Deconvolution was performed as in Fig. 3. (E) Selected 3D rendered iso-surface views are shown and can be viewed in supplementary material Movie 11. (F) CHO-K1 cells expressing paxillin-EGFP were imaged as in Fig. 2. An Olympus TIRF illumination system was used and lasers were attenuated with an AOTF (Prairie Technologies, Middleton, WI). EGFP was excited with ~3% of the 488-nm laser line of a 200-mW Ar laser and Draq5 was excited with ~50% of a 5-mW 633-nm laser. A custom triple dichroic mirror and triple BP emission filter were used (Chroma Technology). Images were collected with a 1-second exposure with no camera binning. The laser was tuned to go straight through the sample for the wide-field images (F) and at the crucial angle for TIRF images (G). Color overlays of WFM and TIRFM images were done using MetaMorph. Images were filtered with a median filter to reduce noise. (H) Intensity profile of paxillin-EGFP signal for five parallel lines averaged from the wide-field image (red line) and the TIRF image (blue line) showing the increase in signal versus background for the TIRF image. (I) Time-lapse images of paxillin-EGFP expressed in CHO-K1 cells, showing a cell rounding up and disappearing from the TIRF field during cell division (panel 4). All display properties (brightness, gamma, contrast) have the same settings for images within a panel. Scale bars: 10 µm.

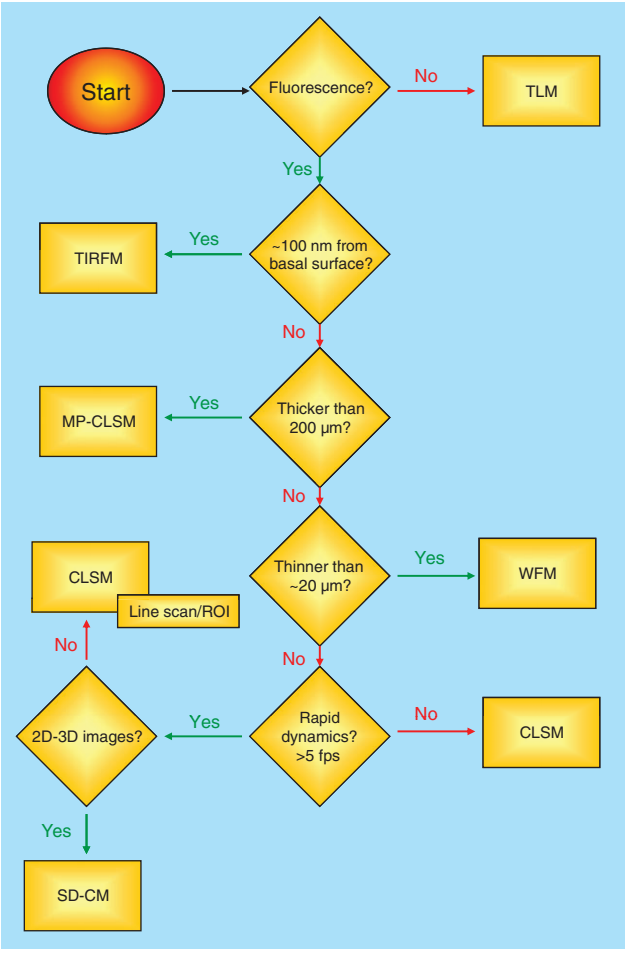

Fig. 6. Suggestions for selection of imaging platform on the basis of sample type, requirement for 3D imaging, and the speed of the dynamics under study. TLM, transmission light microscopy.

improve image quality (e.g. Quorum Technologies). Standard scientific-grade CCD cameras produce beautiful images and, in most cases, can be binned 2×2 to increase the S/N and reduce exposure time. However, to take full advantage of the spinning-disk systems, it is best to equip them with highly sensitive back-thinned EM-CCD cameras, with which imaging speeds can reach video rate for full-frame imaging, or into the hundreds of frames per second with small regions of interest. If 512×512 EM-CCD arrays are used at high magnification (e.g. 60×), there must be additional optical coupling between the camera and the microscope to produce high-resolution images; however, high-quality optics are required to minimize light loss. Post-acquisition blind deconvolution improves SD-CM data, giving superior resolution and a higher S/N relative to the raw data (compare Fig. 5C with 5D). SD-CM data can also be processed, generating beautiful and informative high-resolution 3D reconstruction images (Fig. 5C,D) and movies (Fig. 5E; supplementary material Movie 11) of FPs during membrane ruffling.

Laser light is spread over thousands of pinholes, resulting in focused laser light that is orders of magnitude lower in power at the sample than in CLSM. Each position is sampled hundreds or thousands of times depending on the speed of the disk spinning and the camera's exposure time. The laser passes through the pinholes so that, unlike in CLSM, the excitation light is also confocal, only exciting fluorescence within a small confocal volume rather than through the whole sample. The reduction in photobleaching and phototoxicity with SD-CM is substantial (Wang et al., 2005). In Fig. 5, 28 *z*-axis image planes were collected every 20 seconds for 30 minutes, resulting in virtually continuous sampling. Over 300 seconds (~eight times longer than in Fig. 3B), there is no apparent photobleaching of the FP (Fig. 5A,B). Of course, light levels should still be kept to a minimum (Table 1) because, after 30 minutes of continuous illumination, about 20% of the fluorescence signal is lost (not shown). In general, cells can be imaged extensively for many days on the SD platform (48 hours, seven *z*-planes every 15 minutes) with no obvious effects on cell health or proliferation (Fig. 1C). Owing to the extensive reduction in light exposure when imaging using SD-CM, it is more feasible to collect 3D time-series data of live cells.

Total internal reflection fluorescence microscopy (TIRFM)

TIRFM (also known as evanescent wave microscopy) (Axelrod, 2001; Axelrod, 2003; Trache and Meininger, 2008), is ideal for the study of cell adhesion and migration (Adams et al., 2004; Choi et al., 2008; Nayal et al., 2006), as well as exocytosis (Nagamatsu and Ohara-Imaizumi, 2008) and endocytosis (Schneckenburger, 2005). However, care must be taken when working with confluent cell monolayers because artifacts can be introduced in the TIRF illumination, presumably owing to the high refractive index of the cell monolayer (C.M.B., unpublished observation).

Use TIRF-specific filters to avoid laser-light reflections and interference patterns, and broad BP or LP filters when possible. Similar to SD-CM, choose the appropriate camera on the basis of the need for high spatial resolution (scientific grade CCD) or speed (EM-CCD). There is an inherent increase in signal over background owing to the lack of out-of-focus fluorescence excitation. It is important to note that there is reduced phototoxicity because only the molecules within ~100 nm of the cover glass are excited.

The specificity for the basal surface of the cell is evident from the lack of nuclear staining in the TIRF field (compare Draq5 in Fig. 5F with that in 5G), and there is a significant improvement in the S/N for paxillin-EGFP-containing adhesions (Fig. 5H). Cells move, grow and divide well under TIRF illumination (Fig. 5I; supplementary material Movie 12), with cells disappearing from the TIRF field when rounding up to divide (Fig. 5I, panel 4).

Biophysical tools

There are a tremendous number of biophysical probes, from colorful FPs to organelle-specific dyes, and molecular highlighters available to researchers for live-cell microscopy. We are just scratching the surface with the suggestions provided (Box 2). These probes can be used in combination with photo-activation or fluorescence recovery after photobleaching (FRAP) and other bleaching techniques (Snapp et al., 2003), but care must be taken to ensure that the cells are not exposed to unnecessary amounts of light. Try using one photobleaching scan and see whether it is sufficient to measure protein kinetics. Perhaps looking at the shape of the recovery curve when only 20% of the proteins are bleached is enough. Cell viability should be monitored before, during and after these invasive types of measurements.

Fluorescence-correlation spectroscopy (FCS) (Kim et al., 2007) and ICM (Brown et al., 2008; Wiseman et al., 2004) techniques have been optimized for live-cell microscopy. The ICM tools can be used to map out protein dynamics, concentrations, co-dynamics

Box 2. Fluorescence tools for live-cell imaging

Fluorescent proteins (FPs) and highlighters

There are many reviews dealing with how to choose appropriate FPs with the full spectrum of colors (Day and Schaufele, 2008; Goldman and Spector, 2005; Shaner et al., 2005; Tsien, 2005). Monomeric EGFP is still the FP of choice (monomeric mutation A206K) (Zacharias et al., 2002); however, expression should be maintained at levels similar to those of the endogenous protein. The brightest and most photostable FPs that are most commonly used include: mCitrine (Griesbeck et al., 2001), venus-YFP (Nagai et al., 2002) or the optimal FRET pair of CyPet and YPet (Nguyen and Daugherty, 2005); Kusabira orange (KO) (Karasawa et al., 2004); tdTomato (Shaner et al., 2005); and the newly developed teal FP (TFP) (Ai et al., 2006).

Photo-activatable (PA) and photo-switchable (PS) proteins allow the local demarcation of cells or sub-cellular populations of proteins. For example, PA-EGFP brightens 100 times with 413-nm illumination (Patterson and Lippincott-Schwartz, 2002). Kaede is a tetrameric protein that is switched from green to red in a graded fashion with UV excitation (Ando et al., 2002). Dronpa is a reversibly switchable green FP that can repeatedly be turned on with light at a wavelength of 400 nm and rapidly photoswitched 'off' with an excitation wavelength of 490 nm (Ando et al., 2004). The photo-physical properties of some of these proteins have been characterized (Stark and Kulesa, 2007) and reviewed (Lukyanov et al., 2005). Note that cell health must be monitored when applying UV-light sources to living cells.

Fluorescent probes

Numerous fluorescent compounds are available to detect cellular structures, including the cell-permeant MitoTracker, ER-Tracker and LysoTracker dyes (Invitrogen). Draq5 is a far-red nuclear stain (BioStatus) that is preferable to Hoechst. In general, the smallest amount of reagent possible should be used – often 10-100× more-dilute concentrations than recommended result in good labeling, reduced phototoxicity and reduced cell toxicity that is caused by the presence of the dye. FP constructs that are fused to signaling sequences targeted to various sub-cellular domains can be used either as baculovirus (Organelle Lights, Invitrogen) or as mammalian expression vectors (Simpson et al., 2000; VanEngelenburg and Palmer, 2008). Some of these probes (e.g. FM4-64) are difficult to use with TIRFM because they adhere to the glass, resulting in a very high signal. Adding 5% BSA in the labeling medium will help reduce this non-specific binding.

Biosensors

The field of biosensors is growing rapidly (Hodgson et al., 2008; Li et al., 2006). Some of the many sensors that are available include ratiometric Ca^{2+} sensors such as Fura-2AM (Invitrogen) or FRET-based FPs such as Premo-Cameleon (Invitrogen). Acidity can be measured with pH-sensitive FPs (Patterson et al., 2001) or dye molecules (BCECF, Invitrogen). Chloride concentrations can be monitored using halide-sensitive YFP (Jayaraman et al., 2000). Ion-specific sensors are available from Invitrogen and individual laboratories. Sensors are available for specific phosphorylation events and protease cleavage (Rizzo and Piston, 2005). FRET-based biosensor probes that are even more specific and sophisticated have been developed, for example, for the Rho family of proteins including Cdc42 (Nalbant et al., 2004) and Rac (Kraynov et al., 2000; Pertz and Hahn, 2004).

and colocalization across the living cell. ICM is well-suited to live-cell microscopy because, in contrast to photobleaching techniques, it does not depend on photodamage. However, these techniques can be difficult to master.

Conclusion and perspectives

All of the above platforms can be optimized for live-cell microscopy, and each has its use, depending on the sample type to be imaged and the speed of the cellular processes of interest (Fig. 6). Ensuring that optical light paths are optimized for sensitivity and throughput and that the most sensitive detectors are used will allow for imaging conditions that minimize phototoxicity and maintain cell viability. Live-cell microscopy research is growing exponentially, giving researchers ever-clearer views of the inner workings of the cell. Further improvements to FPs, more-diverse molecular highlighters (Stark and Kulesa, 2007), and the ability to locally photo-uncage and activate molecules (Judkewitz et al., 2006) give researchers a diverse array of tools to follow dynamics within the cell. This, taken together with advances in optical microscopy, PMT and CCD-camera sensitivity and the availability of diverse imaging platforms, will allow the field of live-cell microscopy to continue to grow at an amazing pace. Perhaps, with the development of ultra-high-resolution imaging techniques (Lippincott-Schwartz and Manley, 2009; Fernandez-Suarez and Ting, 2008) that are compatible with rapid live-cell imaging, we will be able to watch the intricate molecular dynamics and interactions within the cell in great detail. Using live-cell imaging, researchers will continue to gain insight into the vast array of cellular processes at work from the single-cell level to their function within the entire organism.

A special thanks to Cory Glowinski from Bitplane for his tireless efforts deconvolving and generating a vast number of 3D rendered images using the Imaris software for Figs 3 and 5. The versatility and immense number and type of visualization tools provided by the software could have been overwhelming without his expertise and guidance. Thank you to David Hitrys from QImaging for his critical reading of the manuscript, his suggestions and interesting discussions. All images in the paper were collected at either the Cell Imaging and Analysis Network (CIAN) or the McGill Imaging Facility, both of which are funded by the Canadian Foundation for Innovation.

References

Adams, M. C., Matov, A., Yarar, D., Gupton, S. L., Danuser, G. and Waterman-Storer, C. M. (2004). Signal analysis of total internal reflection fluorescent speckle microscopy (TIR-FSM) and wide-field epi-fluorescence FSM of the actin cytoskeleton and focal adhesions in living cells. *J. Microsc.* **216**, 138-152.

Ai, H. W., Henderson, J. N., Remington, S. J. and Campbell, R. E. (2006). Directed evolution of a monomeric, bright and photostable version of Clavularia cyan fluorescent protein: structural characterization and applications in fluorescence imaging. *Biochem. J.* **400**, 531-540.

Ando, R., Hama, H., Yamamoto-Hino, M., Mizuno, H. and Miyawaki, A. (2002). An optical marker based on the UV-induced green-to-red photoconversion of a fluorescent protein. *Proc. Natl. Acad. Sci. USA* **99**, 12651-12656.

Ando, R., Mizuno, H. and Miyawaki, A. (2004). Regulated fast nucleocytoplasmic shuttling observed by reversible protein highlighting. *Science* **306**, 1370-1373.

Axelrod, D. (2001). Total internal reflection fluorescence microscopy in cell biology. *Traffic* **2**, 764-774.

Axelrod, D. (2003). Total internal reflection fluorescence microscopy in cell biology. *Methods Enzymol.* **361**, 1-33.

Boivin, B., Villeneuve, L. R., Farhat, N., Chevalier, D. and Allen, B. G. (2005). Sub-cellular distribution of endothelin signaling pathway components in ventricular myocytes and heart: lack of preformed caveolar signalosomes. *J. Mol. Cell Cardiol.* **38**, 665-676.

Bolte, S. and Cordelieres, F. P. (2006). A guided tour into subcellular colocalization analysis in light microscopy. *J. Microsc.* **224**, 213-232.

Brown, C. M. (2007). Fluorescence microscopy-avoiding the pitfalls. *J. Cell Sci.* **120**, 1703-1705.

Brown, C. M., Dalal, R. B., Hebert, B., Digman, M. A., Horwitz, A. R. and Gratton, E. (2008). Raster image correlation spectroscopy (RICS) for measuring fast protein dynamics and concentrations with a commercial laser scanning confocal microscope. *J. Microsc.* **229**, 78-91.

Cardullo, R. A. and Hinchcliffe, E. H. (2007). Digital manipulation of brightfield and fluorescence images: noise reduction, contrast enhancement, and feature extraction. *Methods Cell Biol.* **81**, 285-314.

Casey, J. R. (2006). Why bicarbonate? *Biochem. Cell Biol.* **84**, 930-939.
Choi, C. K., Vicente-Manzanares, M., Zareno, J., Whitmore, L. A., Mogilner, A. and Horwitz, A. R. (2008). Actin and alpha-actinin orchestrate the assembly and maturation of nascent adhesions in a myosin II motor-independent manner. *Nat. Cell Biol.* **10**, 1039-1050.
Comeau, J. W., Costantino, S. and Wiseman, P. W. (2006). A guide to accurate fluorescence microscopy colocalization measurements. *Biophys. J.* **91**, 4611-4622.
Cornell-Bell, A. H. and Finkbeiner, S. M. (1991). Ca^{2+} waves in astrocytes. *Cell Calcium* **12**, 185-204.
Dailey, M. E., Manders, E., Soll, D. R. and Terasaki, M. (2006). Confocal microscopy of living cells. In *Handbook of Biological Confocal Microscopy* (ed. J. Pawley), pp. 381-403. New York: Springer.
Day, R. N. and Schaufele, F. (2005). Imaging molecular interactions in living cells. *Mol. Endocrinol.* **19**, 1675-1686.
Day, R. N. and Schaufele, F. (2008). Fluorescent protein tools for studying protein dynamics in living cells: a review. *J. Biomed. Opt.* **13**, 031202.
Digman, M. A., Brown, C. M., Horwitz, A. R., Mantulin, W. W. and Gratton, E. (2008). Paxillin dynamics measured during adhesion assembly and disassembly by correlation spectroscopy. *Biophys. J.* **94**, 2819-2831.
Fernandez-Suarez, M. and Ting, A. Y. (2008). Fluorescent probes for super-resolution imaging in living cells. *Nat. Rev. Mol. Cell. Biol.* **9**, 929-943.
Fraser, S. E. and O'Rourke, N. A. (1990). In situ analysis of neuronal dynamics and positional cues in the patterning of nerve connections. *J. Exp. Biol.* **153**, 61-70.
Goldman, R. D. and Spector, D. L. (2005). *Live Cell Imaging: A Laboratory Manual*. Cold Spring Harbor, NY: Cold Spring Harbor Laboratory Press.
Griesbeck, O., Baird, G. S., Campbell, R. E., Zacharias, D. A. and Tsien, R. Y. (2001). Reducing the environmental sensitivity of yellow fluorescent protein. Mechanism and applications. *J. Biol. Chem.* **276**, 29188-29194.
Haraguchi, T. (2002). Live cell imaging: approaches for studying protein dynamics in living cells. *Cell Struct. Funct.* **27**, 333-334.
Helmchen, F. and Denk, W. (2005). Deep tissue two-photon microscopy. *Nat. Methods* **2**, 932-940.
Hibbs, A. (2004). *Confocal Microscopy for Biologists*. New York: Springer.
Hodgson, L., Pertz, O. and Hahn, K. M. (2008). Design and optimization of genetically encoded fluorescent biosensors: GTPase biosensors. *Methods Cell Biol.* **85**, 63-81.
Holmes, T. J., Biggs, D. and Abu-Tarif, A. (2006). Blind deconvolution. In *Handbook of Biological Confocal Microscopy* (ed. J. Pawley), pp. 468-487: New York: Springer.
Ichihara, A., Tanaami, T., Isozaki, K., Sugiyama, Y., Kosugi, Y., Mikuriya, K., Abe, M. and Uemura, I. (1996). High speed confocal fluorescence microscopy using a nipkow scanner with microlenses for 3d imaging of single fluorescent molecule in real time. *Bioimages* **4**, 52-62.
Jayaraman, S., Haggie, P., Wachter, R. M., Remington, S. J. and Verkman, A. S. (2000). Mechanism and cellular applications of a green fluorescent protein-based halide sensor. *J. Biol. Chem.* **275**, 6047-6050.
Judkewitz, B., Roth, A. and Hausser, M. (2006). Dendritic enlightenment: using patterned two-photon uncaging to reveal the secrets of the brain's smallest dendrites. *Neuron* **50**, 180-183.
Kanaan, A., Douglas, R. M., Alper, S. L., Boron, W. F. and Haddad, G. G. (2007). Effect of chronic elevated carbon dioxide on the expression of acid-base transporters in the neonatal and adult mouse. *Am. J. Physiol. Regul. Integr. Comp. Physiol.* **293**, R1294-R1302.
Karasawa, S., Araki, T., Nagai, T., Mizuno, H. and Miyawaki, A. (2004). Cyan-emitting and orange-emitting fluorescent proteins as a donor/acceptor pair for fluorescence resonance energy transfer. *Biochem. J.* **381**, 307-312.
Kawano, H., Kogure, T., Abe, Y., Mizuno, H. and Miyawaki, A. (2008). Two-photon dual-color imaging using fluorescent proteins. *Nat. Methods* **5**, 373-374.
Kim, S. A., Heinze, K. G. and Schwille, P. (2007). Fluorescence correlation spectroscopy in living cells. *Nat. Methods* **4**, 963-973.
Knight, M. M., Roberts, S. R., Lee, D. A. and Bader, D. L. (2003). Live cell imaging using confocal microscopy induces intracellular calcium transients and cell death. *Am. J. Physiol. Cell Physiol.* **284**, C1083-C1089.
Konig, K. (2006). Cell damage during multi-photon microscopy. In *Handbook of Biological Confocal Microscopy* (ed. J. Pawley), pp. 680-689. New York: Springer.
Kraus, B., Zeigler, M. and Wolff, H. (2007). Linear fluorescence unmixing in cell biological research. In *Modern Research and Educational Topics in Microscopy*. Vol. 2, (ed. A. Mendez-Vilas and J. Diaz), pp. 863-873. Badajoz, Spain: Formatex Microscopy Book Series.
Kraynov, V. S., Chamberlain, C., Bokoch, G. M., Schwartz, M. A., Slabaugh, S. and Hahn, K. M. (2000). Localized Rac activation dynamics visualized in living cells. *Science* **290**, 333-337.
Li, I. T., Pham, E. and Truong, K. (2006). Protein biosensors based on the principle of fluorescence resonance energy transfer for monitoring cellular dynamics. *Biotechnol. Lett.* **28**, 1971-1982.
Lichtman, J. W. and Conchello, J. A. (2005). Fluorescence microscopy. *Nat. Methods* **2**, 910-919.
Lippincott-Schwartz, J. and Manley, S. (2009). Putting super-resolution fluorescence microscopy to work. *Nat. Methods* **6**, 21-23.
Lukyanov, K. A., Chudakov, D. M., Lukyanov, S. and Verkhusha, V. V. (2005). Innovation: photoactivatable fluorescent proteins. *Nat. Rev. Mol. Cell. Biol.* **6**, 885-891.
McNally, J. G., Karpova, T., Cooper, J. and Conchello, J. A. (1999). Three-dimensional imaging by deconvolution microscopy. *Methods* **19**, 373-385.
Mueller, M. (2005). *Introduction to Confocal Fluorescence Microscopy*. Bellingham, WA: SPIE Publications.
Murphy, D. (2001). *Fundamentals of Light Microscopy and Electronic Imaging*. Canada: John Wiley.
Murray, J. M. (2005). Confocal microscopy, deconvolution, and structured illumination methods. In *Live Cell Imaging: A Laboratory Manual* (ed. R. D. Goldman and D. L. Spector), pp. 239-279. Cold Spring Harbor, NY: Cold Spring Harbor Laboratory Press.
Murray, J. M. (2007). Practical aspects of quantitative confocal microscopy. *Methods Cell Biol.* **81**, 467-478.
Nagai, T., Ibata, K., Park, E. S., Kubota, M., Mikoshiba, K. and Miyawaki, A. (2002). A variant of yellow fluorescent protein with fast and efficient maturation for cell-biological applications. *Nat. Biotechnol.* **20**, 87-90.
Nagamatsu, S. and Ohara-Imaizumi, M. (2008). Imaging exocytosis of single insulin secretory granules with TIRF microscopy. *Methods Mol. Biol.* **440**, 259-268.
Nalbant, P., Hodgson, L., Kraynov, V., Toutchkine, A. and Hahn, K. M. (2004). Activation of endogenous Cdc42 visualized in living cells. *Science* **305**, 1615-1619.
Nayal, A., Webb, D. J., Brown, C. M., Schaefer, E. M., Vicente-Manzanares, M. and Horwitz, A. R. (2006). Paxillin phosphorylation at Ser273 localizes a GIT1-PIX-PAK complex and regulates adhesion and protrusion dynamics. *J. Cell Biol.* **173**, 587-589.
Nguyen, A. W. and Daugherty, P. S. (2005). Evolutionary optimization of fluorescent proteins for intracellular FRET. *Nat. Biotechnol.* **23**, 355-360.
Nordberg, J. J. and Sluder, G. (2007). Practical aspects of adjusting digital cameras. *Methods Cell Biol.* **81**, 159-169.
North, A. J. (2006). Seeing is believing? A beginners' guide to practical pitfalls in image acquisition. *J. Cell Biol.* **172**, 9-18.
Nyquist, H. (1928). Certain topics in telegraph transmission theory. *Trans. AIEE* **47**, 617-644.
Oheim, M., Michael, D. J., Geisbauer, M., Madsen, D. and Chow, R. H. (2006). Principles of two-photon excitation fluorescence microscopy and other nonlinear imaging approaches. *Adv. Drug Deliv. Rev.* **58**, 788-808.
Patterson, G. H. and Piston, D. W. (2000). Photobleaching in two-photon excitation microscopy. *Biophys. J.* **78**, 2159-2162.
Patterson, G. H. and Lippincott-Schwartz, J. (2002). A photoactivatable GFP for selective photolabeling of proteins and cells. *Science* **297**, 1873-1877.
Patterson, G., Day, R. N. and Piston, D. (2001). Fluorescent protein spectra. *J. Cell Sci.* **114**, 837-838.
Pattison, D. I. and Davies, M. J. (2006). Actions of ultraviolet light on cellular structures. *EXS* 131-157.
Pawley, J. (2006). *Handbook of Biological Confocal Microscopy*. New York: Springer.
Pertz, O. and Hahn, K. M. (2004). Designing biosensors for Rho family proteins-deciphering the dynamics of Rho family GTPase activation in living cells. *J. Cell Sci.* **117**, 1313-1318.
Piston, D. W. (2006). The coming of age of two-photon excitation imaging for intravital microscopy. *Adv. Drug Deliv. Rev.* **58**, 770-772.
Rizzo, M. A. and Piston, D. W. (2005). Fluorescent protein tracking and detection. In *Live Cell Imaging: A Laboratory Manual* (ed. R. D. Goldman and D. L. Spector), pp. 3-23. Cold Spring Harbor, NY: Cold Spring Harbor Laboratory Press.
Rocheleau, J. V. and Piston, D. W. (2003). Two-photon excitation microscopy for the study of living cells and tissues. *Curr. Protoc. Cell Biol.* **Chapter 4**, Unit 4 11.
Schneckenburger, H. (2005). Total internal reflection fluorescence microscopy: technical innovations and novel applications. *Curr. Opin. Biotechnol.* **16**, 13-18.
Schwille, P., Haupts, U., Maiti, S. and Webb, W. W. (1999). Molecular dynamics in living cells observed by fluorescence correlation spectroscopy with one- and two-photon excitation. *Biophys. J.* **77**, 2251-2265.
Shaner, N. C., Steinbach, P. A. and Tsien, R. Y. (2005). A guide to choosing fluorescent proteins. *Nat2 Methods* **2**, 905-909.
Shannon, C. E. (1949). Communication in the presence of noise. *Proc. Inst. Radio Eng.* **37**, 10-21.
Shaw, P. J. (2006). Comparison of widefield/deconvolution and confocal microscopy for three-dimensional imaging. In *Handbook of Biological Confocal Microscopy* (ed. J. Pawley), pp. 453-467. New York: Springer.
Sheftel, A. D., Zhang, A. S., Brown, C., Shirihai, O. S. and Ponka, P. (2007). Direct interorganellar transfer of iron from endosome to mitochondrion. *Blood* **110**, 125-132.
Simpson, J. C., Wellenreuther, R., Poustka, A., Pepperkok, R. and Wiemann, S. (2000). Systematic subcellular localization of novel proteins identified by large-scale cDNA sequencing. *EMBO Rep.* **1**, 287-292.
Snapp, E. L., Altan, N. and Lippincott-Schwartz, J. (2003). Measuring protein mobility by photobleaching GFP chimeras in living cells. *Curr. Protoc. Cell Biol.* **Chapter 21**, Unit 21 1.
Spring, K. R. (2007). Cameras for digital microscopy. *Methods Cell Biol.* **81**, 171-186.
Standish, B. (2008). High performance with fluorescence optical filters. *BioOptics World* **September/October**, 35-37.
Stark, D. A. and Kulesa, P. M. (2007). An in vivo comparison of photoactivatable fluorescent proteins in an avian embryo model. *Dev. Dyn.* **236**, 1583-1594.
Suen, D. F., Norris, K. L. and Youle, R. J. (2008). Mitochondrial dynamics and apoptosis. *Genes Dev.* **22**, 1577-1590.
Swedlow, J. R. (2007). Quantitative fluorescence microscopy and image deconvolution. *Methods Cell Biol.* **81**, 447-465.
Toomre, D. and Pawley, J. B. (2006). Disk scanning confocal microscopy. In *Handbook of Biological Confocal Microscopy* (ed. J. Pawley), pp. 221-238. New York: Springer.
Trache, A. and Meininger, G. A. (2008). Total internal reflection fluorescence (TIRF) microscopy. *Curr. Protoc. Microbiol.* **Chapter 2**, Unit 2A.2.1-2A.2.22.
Tsien, R. Y. (2005). Building and breeding molecules to spy on cells and tumors. *FEBS Lett.* **579**, 927-932.

VanEngelenburg, S. B. and Palmer, A. E. (2008). Fluorescent biosensors of protein function. *Curr. Opin. Chem. Biol.* **12**, 60-65.
Wallace, W., Schaefer, L. H. and Swedlow, J. R. (2001). A workingperson's guide to deconvolution in light microscopy. *Biotechniques* **31**, 1076-1078; 1080; 1082; passim.
Wang, E., Babbey, C. M. and Dunn, K. W. (2005). Performance comparison between the high-speed Yokogawa spinning disc confocal system and single-point scanning confocal systems. *J. Microsc.* **218**, 148-159.
Wang, Y., Shyy, J. Y. and Chien, S. (2008). Fluorescence proteins, live-cell imaging, and mechanobiology: seeing is believing. *Annu. Rev. Biomed. Eng.* **10**, 1-38.
Webb, D. J., Parsons, J. T. and Horwitz, A. F. (2002). Adhesion assembly, disassembly and turnover in migrating cells-over and over and over again. *Nat. Cell Biol.* **4**, E97-E100.
Webb, D. J., Donais, K., Whitmore, L. A., Thomas, S. M., Turner, C. E., Parsons, J. T. and Horwitz, A. F. (2004). FAK-Src signalling through paxillin, ERK and MLCK regulates adhesion disassembly. *Nat. Cell Biol.* **6**, 154-161.
Wiseman, P. W., Squier, J. A., Ellisman, M. H. and Wilson, K. R. (2000). Two-photon image correlation spectroscopy and image cross-correlation spectroscopy. *J. Microsc.* **200**, 14-25.
Wiseman, P. W., Brown, C. M., Webb, D. J., Hebert, B., Johnson, N. L., Squier, J. A., Ellisman, M. H. and Horwitz, A. F. (2004). Spatial mapping of integrin interactions and dynamics during cell migration by image correlation microscopy. *J. Cell Sci.* **117**, 5521-5534.
Wolf, D. E. (2007). Fundamentals of fluorescence and fluorescence microscopy. *Methods Cell Biol.* **81**, 63-91.
Wolf, D. E., Samarasekera, C. and Swedlow, J. R. (2007). Quantitative analysis of digital microscope images. *Methods Cell Biol.* **81**, 365-396.
Yamaguchi, H., Wyckoff, J. and Condeelis, J. (2005). Cell migration in tumors. *Curr. Opin. Cell Biol.* **17**, 559-564.
Zacharias, D. A., Violin, J. D., Newton, A. C. and Tsien, R. Y. (2002). Partitioning of lipid-modified monomeric GFPs into membrane microdomains of live cells. *Science* **296**, 913-916.

Journal of Cell Science